Journal of Materials, Processing and Design (2025)
Clausius Scientific Press, Canada

DOI: 10.23977/jmpd.2025.090108
ISSN 2516-0923 Vol. 9 Num. 1

Tribo-corrosion behaviors of plasma sprayed ceramic coating in hydrochloric acid

Nairu He, Jintao Qiu, Jie Yang*

College of Mechanical and Electrical Engineering, Shaanxi University of Science & Technology, Xi'an, 710021, China
**Corresponding author*

Keywords: Plasma spray; TiO_2; coating; tribo-corrosion

Abstract: This study employed atmospheric plasma spraying (APS) technology to fabricate TiO_2 coatings on 310S stainless steel substrates, systematically investigating their corrosion-wear mechanisms under dry friction, deionized water, and 5% HCl solution environments. Experimental results revealed that under high contact stress, the coatings exhibited significantly enhanced tribological performance, with stable coefficients of friction (COF) in the ranges of 0.4–0.5 (dry friction), 0.2–0.3 (deionized water), and 0.18 (5% HCl solution). Quantitative wear rate analysis demonstrated a substantial reduction in the coating's volumetric wear rates compared to the substrate, measuring 7.18×10^{-6} mm³/(N·m), 9.20×10^{-7} mm³/(N·m), and 1.59×10^{-6} mm³/(N·m) in the respective environments, corresponding to reductions by factors of 2.45, 1.18, and 22.58. Despite the presence of micro-pores and cracks that induced a negative shift in the open-circuit potential within Cl^--containing media, the dense TiO_2 coating effectively mitigated corrosive ion penetration, reduced corrosion current density, and improved corrosion resistance.

1. Introduction

In the chemical field, engineering equipment and its key components are subjected to the synergistic effect of wear and corrosion for a long time, and this double damage mechanism often leads to premature failure of components. Pumps and valves, as critical moving parts widely used in industrial applications, play a key role in chemical processing, petroleum refining, and marine engineering[1]. Although the domestic pump and valve manufacturing technology has made significant progress, in the high-end market is still facing many challenges, in which the valve body and valve seat sealing mate damage is particularly prominent, which is also one of the main reasons why China's high-end pump and valve long-term dependence on imports. In actual working conditions, when the valve is frequently opened and closed, the valve body and valve seat are often in the boundary lubrication or even dry friction state, which is very easy to cause serious friction and wear problems. More seriously, these key components are not only subjected to mechanical friction and wear and tear tests, but also subjected to the corrosion of chemical media at the same time. During the friction process, the passivation film on the surface of the material is constantly destroyed. This exposes the fresh material surface to corrosive fluids continuously, exacerbating the

corrosion process. Ultimately, this forms a synergistic effect of wear and corrosion.[2, 3]. Therefore, the development of protective coatings with excellent wear resistance and corrosion resistance is of great practical significance in extending the service life of engineering equipment in harsh environments.

Based on the above working conditions, the friction sub-materials must have both excellent wear resistance and corrosion resistance. Metal-ceramic oxides have been widely used in the industrial field due to their excellent chemical stability, high hardness, and wear resistance[4, 5]. which provide a reliable guarantee for the stable operation of critical structures in harsh environments. As an important surface engineering technology, thermal spraying technology can give excellent performance to the substrate material by preparing functional protective coatings on the surface of the material, which is not available in the substrate material itself[6]. Among these technologies, plasma spraying has become the most widely researched, developed, and applied method. This is due to its use of high-temperature, high-speed plasma jets with temperatures up to 10,000 ℃ or more as the heat source, which can melt and spray all materials with physical melting points. Especially in the field of preparation of high melting point ceramic coatings, plasma spraying technology shows irreplaceable advantages[7, 8].

In related research, Chengpeng Wang and Xiaobo Wu et al.[9] investigated the friction and wear behavior of alumina ceramics and corrosion-resistant metals under varying environmental media. Their study demonstrated that the friction coefficient was significantly influenced by differences in environmental conditions. In addition, Jin-Kun Xiao et al.[10] successfully prepared NiCrBSi-Zr coatings using atmospheric plasma spraying technology, and it was found that the corrosion resistance of the coatings was closely correlated with porosity. Specifically, the low porosity coatings showed excellent wear and corrosion resistance. S.M. Hashemi et al.[11]evaluated the tribological and corrosion-resistant properties of atmospheric plasma-sprayed Cr_2O_3-20YSZ and Cr_2O_3-20YSZ-10SiC composite coatings on 304L stainless steel substrates in a 3.5wt% NaCl solution. Their study revealed that the protective performance of these coatings was strongly dependent on their porosity characteristics.

Among many metal-ceramic oxides, TiO_2 ceramic coatings are distinguished by their very low porosity, excellent wear resistance, superior chemical stability, good toughness, and ease of processing. In addition, the coating has a low surface roughness and exhibits excellent corrosion resistance to most acids, salts, and other solvents[12]. Therefore, it is considered an important corrosion- and wear-resistant coating material. However, the current research on titanium oxide coatings under corrosion-wear coupling in the chemical industry is still relatively limited. To address this gap, titanium oxide coatings were prepared on the surface of a 310S stainless steel substrate using atmospheric plasma spraying technology. The friction and wear behaviours of the coatings and the substrate were systematically investigated in dry friction and deionized water environments. Furthermore, the corrosion and wear behaviours in a 5% HCl solution were explored. By analysing the tribological behaviours of TiO_2 ceramic coating and different friction partners under different contact stresses, this study aims to aim to determine the optimal combination of friction partners, which will provide a theoretical basis and practical guidance for the selection of materials under corrosive-wear coupling conditions in the chemical industry.

2. Experimental Method

2.1. Experimental materials

For this test, 310S stainless steel was selected as the substrate material, and its size specification was Φ30 mm × 8 mm cylindrical steel sheet. Before spraying, the oxides on the surface of the substrate were firstly abraded and polished, and then the treated samples were placed in anhydrous

ethanol solution and ultrasonically cleaned for 10 minutes in order to completely remove the surface oil. The cleaned samples were placed in a blast drying oven for drying. In order to enhance the bonding strength between the coating and the substrate, the surface of the substrate was roughened using sandblasting equipment (Model: JCK-1010A, Shanghai Jichuan Machinery Technology Co., Ltd.). The sandblasting pressure was controlled at 0.6~0.8 MPa, and the sand grain size was 80~120 mesh.

2.2. Coating Preparation

The spraying experiments were conducted using atmospheric plasma spraying equipment (Model: APS-3000K, manufactured by China Academy of Aeronautical Technology). The particle sizes of NiAl powder and TiO_2 powder used for spraying were 40-60μm and 30-45μm, respectively, their microscopic morphologies are shown in Figure 1. To reduce thermal stress caused by uneven thermal expansion and contraction between the coating and the substrate, the substrate was preheated using a plasma spray gun to a temperature of 200-250 ℃ without feeding the powder before spraying. Spraying was then initiated. During the spraying process, NiAl was first sprayed on the surface of the substrate as a bonding layer with a thickness of 80~100μm, and then TiO_2 coating was sprayed on the bonding layer with a thickness of 280~300μm. The spraying parameters are shown in Table 1.

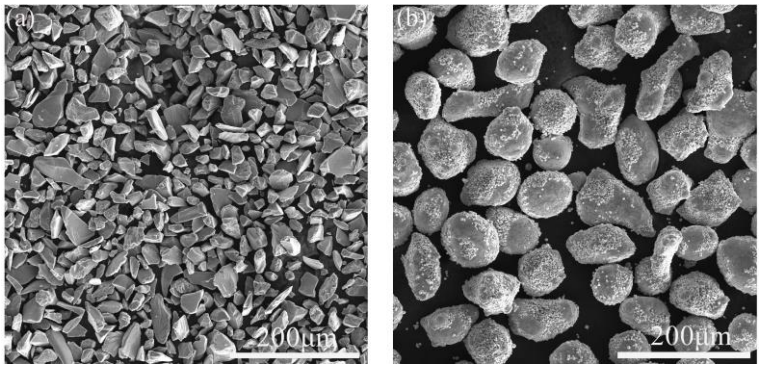

Figure 1: SEM morphology of sprayed powder (a) TiO_2 powder (b) NiAl powder

Table 1: Plasma spraying parameters for the coatings

parametric	TiO_2 coating	NiAl bonded layer
Current (A)	520	520
Voltage (V)	55	62
Ar Flow rate (L/min)	40	55
H_2 Flow rate (L/min)	5	5
Speed (rad/min)	12	15
Spraying distance(mm)	90	80

2.3. Testing Instruments

A microhardness tester (HV-1000A, Laizhou Huayin Testing Instrument Co., Ltd.) was used to measure the microhardness of the coating and 310S substrate. The indenter was a 136 ° positive four-pronged cone, the load was 500 g, and the holding pressure was 15s. Ten points were randomly selected in the coating cross-section, and the average value of the test data was taken as the microVickers hardness value of the coating.

A reciprocating electrochemical friction and wear tester was used for the corrosion friction test.

The load was 5 N, frequency is 2 Hz, and the reciprocating stroke was 5 mm. Different sizes of counterpart balls can produce different stress distributions when in contact. Smaller spheres concentrate stress more, while larger spheres distribute it more evenly. This helps to better understand the behavior, deformation, and fatigue of materials under frictional contact. The counter-abrasive fittings selected for coating were 3mm and 6mm SiC ceramic balls, as well as 6mm 316L balls. When the counter-abrasive fittings of the substrate are 3mm SiC balls, according to the Hertzian contact theory, it can be calculated that the contact stresses of the TiO_2 coating with 3mm SiC are about 2033.69~2660.8Mpa, those of the 6mm SiC are about 1281.5~1676.24Mpa, and those of the 6mm 316L balls are about 888.65~969.59Mpa.

The electrochemical friction experiment was conducted for 70 min. The specimens were immersed in mass fraction 5% HCl for the first 5 min, and the reciprocal friction time was 60 min, followed by 5 min of rest. At the end of the friction, the wear section of the specimens was measured by a non-contact three-dimensional surface profilometer (DSX510, Olympus Co., Ltd.). The wear rate of the coating was calculated by the formula W=V/FL, Where W is the wear rate, V is the wear volume, F is the load and L is the sliding distance.

2.4. Microscopic morphology observation

The morphology of the abrasion marks was observed using a swept electron microscope (SEM) and analysed by a self-contained energy spectrometer (EDS). The phase composition of the powders and coatings was analysed using an X-ray diffractometer with Cu-K radiation (XRD, D8-Discover 25, Bruker, Germany). During the tests, the scanning speed was 10 °/min, the step size was 0.02°, the scanning angle (2θ) ranged from 20° to 80 °, the accelerating voltage was 40 kV, and the current was 20 mA.

3. Experimental results

3.1. TiO_2 powder and coating phase composition and coating cross-section micromorphology

As shown in Fig.2 (a), the XRD pattern analysis of TiO_2 coatings and powders revealed that the physical phase composition of the pristine TiO_2 powders contained rutile and oxygen-deficient phases. During the plasma spraying process, the TiO_2 powder undergoes a significant phase transformation due to the high-temperature flame flow, in which the oxygen-deficient phase is completely transformed into the thermodynamically more stable rutile phase.

As shown in Fig.2 (b), the cross-sectional morphology of the TiO2 coating, examined at 600× magnification using scanning electron microscopy (SEM), reveals a good mechanical interlocking structure between the coating and the metal adhesion layer. The cross-section of the coating exhibits a uniform and dense microstructure. However, a small number of pores and microcracks, typical of thermal spray coatings, are also present. Furthermore, the average thickness of the TiO2 functional layer was determined to be 250 ± 15 μm, while that of the metal adhesion layer was 60 ± 10 μm.

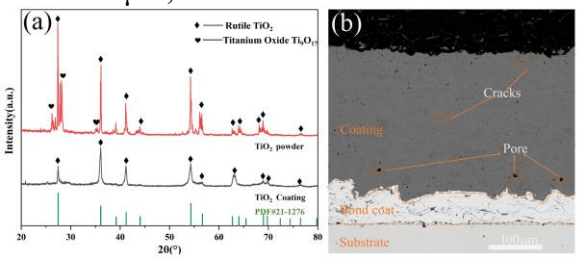

Figure 2 (a) XRD pattern of TiO_2 powder and coating (b) TiO_2 cross-section morphology

3.2. Mechanical properties of coatings

Microhardness is one of the important indexes for evaluating the performance of coatings and is closely related to the wear resistance and service life of coatings[13]. Figure 3 shows the SEM images of the coating indentation and its microhardness value. From the indentation morphology, it can be seen that there is no crack around the indentation due to pressure, which indicates that the coating has excellent fracture toughness. Furthermore, the microhardness value of the 310S substrate is 265.67 HV, while the microhardness value of the coating reaches 1004.57 HV, which is significantly higher than that of the substrate. This further demonstrates that the coating exhibits excellent performance in terms of both hardness and toughness.

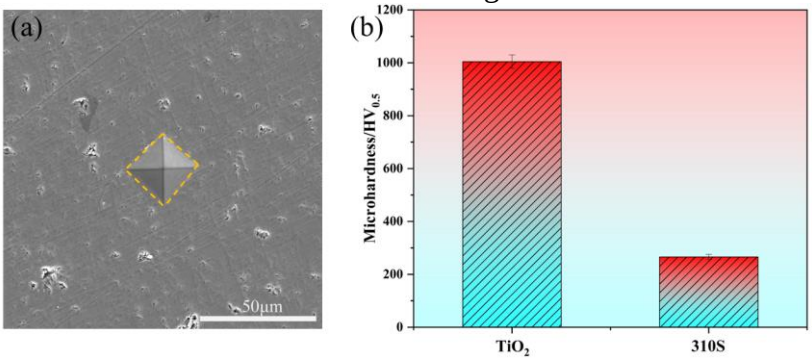

Figure 3: (a) SEM morphology of coating hardness indentation (b) Vickers hardness values of TiO2 and 310S

3.3. Tribological performance of TiO_2 coatings in different environments

Fig.4 demonstrates the friction coefficient profiles of TiO_2 coating and substrate in dry friction, deionised water and HCl environments. Figures (a) and (b) show the friction coefficient profiles of 3 mm SiC and 6 mm SiC Ball with TiO_2 coating in the three environments, respectively. The friction coefficients of 3 mm SiC ball is lower than those of 6 mm SiC ball in all three environments, which are 0.4~0.5, 0.2~0.3, and 0.18, respectively. The friction coefficients of the coatings against the balls are significantly affected by the contact area and the ambient medium. Generally, a larger contact area usually results in a higher friction coefficient. In a dry friction environment, the coefficient of friction of the coating against the 6 mm SiC ball is stable at around 0.8, which is higher than that of the 3 mm SiC ball. In the deionized water environment, the coefficient of friction decreases to 0.62. This reduction is attributed to the lubrication effect of water molecules, which form a lubricating film on the coating surface, thereby reducing friction and lowering the coefficient of friction.

Figure.4(c) shows the coefficient of friction profile of the coating with 6 mm 316L dyadic ball. In dry friction and deionised water environment, the coefficient of friction is higher at 0.75 and 0.6, respectively. This can be attributed to the significant hardness difference between the coating and the 316L counterpart balls. This difference causes the counterpart balls to adhere to the coating surface during friction, resulting in adhesive wear.

In HCl solution, the coefficient of friction decreased significantly to approximately 0.18 for 3 mm SiC counterpart ball, 0.25 for 6 mm SiC counterpart ball, and 0.3 to 0.4 for 6 mm 316L counterpart ball. This may be due to the interaction of Cl- and H^+ with the surface of TiO_2 to form a double electric layer structure. The electric double layer can be divided into two regions: the compact layer near the solid surface and the diffuse layer away from the surface. During friction, the formation of the electric double layer produces an additional lubricating effect at the contact

interface, which significantly reduces the coefficient of friction. Water has a high dielectric constant, but in water, the water molecules do not form a well-defined electric double layer as in HCl, and hence the coefficient of friction is relatively high. The TiO_2 ceramic coatings showed excellent tribological performance in HCl.

Figure.4(d) illustrates the coefficient of friction between the substrate and the 3mm SiC counterpart ball. In dry friction environment, the friction coefficient of the substrate increases rapidly. This can be attributed to the increase in frictional heat caused by higher surface contact stresses during continuous friction, which leads to the softening of the substrate. This softening increases the plastic deformation of the friction surface, thereby reducing the material's shear strength. Consequently, the coefficient of friction decreases and stabilizes at 0.4. In the liquid medium, the wear debris can act as lubricant on the surface of the wear track after being sheared. In addition, in corrosive media, the coefficient of friction of the substrate is significantly influenced by the corrosion products, and the substrate is more easily sheared in corrosive media compared to dry friction environments [14, 15].

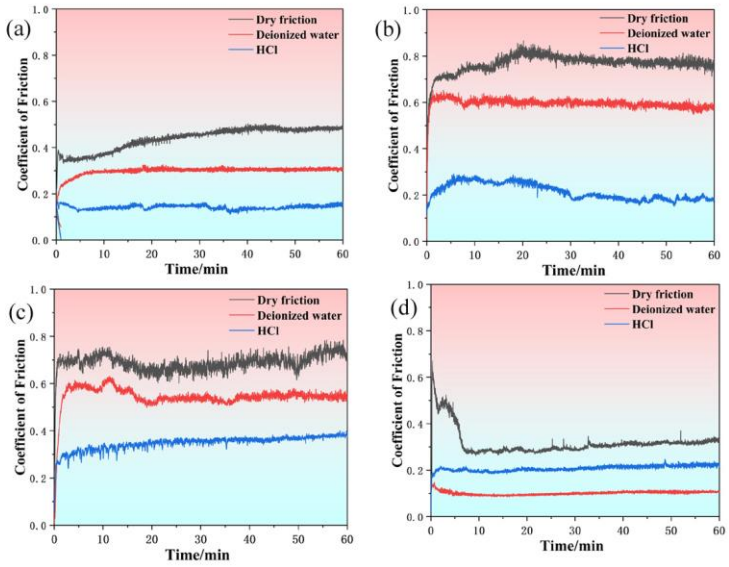

Figure 4: Coefficient of friction curves of coatings and substrates in different environments: (a) with 3mm SiC as counterpart (b) with 6mm SiC as counterpart (c) Coefficient of friction curve of 6mm 316L sliding against TiO_2 (d) 3mm SiC counterpart sliding against 310S

3.4. Wear rate of coatings and couples

3.4.1. Coating wear rate

Figure 5 illustrates the wear rate data of the coating and substrate in different environments. Under high contact stress conditions, the wear rates of the coatings in dry friction, deionised water and HCl environments are 7.18×10^{-6} mm^3/(N·m), 9.20×10^{-7} mm^3/(N·m) and 1.59×10^{-6} mm^3/(N·m); while the wear rates of the coatings in the corresponding environments were 1.33×10^{-6}mm^3/(N·m), 3.94×10^{-6} mm^3/(N·m), and 3.54×10^{-6} mm^3/(N·m) under the low contact stress condition, respectively. Analysing the data, it can be seen that the wear rate of the coatings does not simply increase with increasing contact stress, especially in the deionised water and HCl environments, where the wear rate at low contact stress is instead significantly higher than that at high contact stress. This phenomenon may be closely related to the wear mechanism and media properties in different environments.

In dry friction environments, high contact stresses contribute to TiO_2 coatings under high contact

stresses, and the tips of surface microcracks are susceptible to stress concentrations, which can lead to the rapid expansion of cracks and formation of spalls, and increase the wear rate.

The higher wear rate under low contact stress in deionised water and HCl environments may be related to the characteristics of the liquid medium and its effect on the wear process. Firstly, at low contact stresses, the contact area between the counterpart balls and the coating is larger, and the liquid medium is more likely to penetrate into the contact area, thus increasing the wear. Secondly, the presence of liquid media washes away the abrasive debris generated during friction, resulting in the inability of the abrasive debris to fill the surface defects, which in turn accelerates crack extension and surface damage. In addition, in the HCl environment, the low contact stress prolongs the contact time between the corrosive medium and the coating, and the synergistic effect of chemical corrosion and mechanical wear further increases the wear rate. In contrast, liquid media at high contact stresses may form a lubricating film that reduces direct contact while abrasive debris is rapidly pushed out of the contact area, resulting in lower wear rates.

When the ball is 316L stainless steel, the wear rate of the coating in a dry friction environment was 9.63 × 10-⁵ mm³/(N·m), which was significantly higher than that of the 6 mm SiC ball by two orders of magnitude. This is due to the large difference in hardness between the 316L stainless steel and the coating, resulting in the counterpart balls being prone to adhesion during friction, and the reciprocal friction triggers coating tearing, which significantly increases the wear rate of the coating. However, in the deionised water and HCl environments, the wear rates of the coatings were significantly reduced to 1.04×10-6mm³/(N·m) and 6.3×10^{-7}mm³/(N·m), respectively. In the deionised water environment, the water molecule scouring effect reduced the adhesion of the abrasive chips, while in the HCl environment, the abrasive chips adhering to the coating were corroded and more easily sheared, thus reducing the wear rate.

When the substrate was ground against 3 mm SiC, the wear rate of the substrate was large, which is 1.76×10^{-5}mm^3/(N·m), 1.09×10^{-6}mm^3/(N·m) and 3.59×10^{-5}mm^3/(N·m) in the three environments, respectively. Corrosion accelerates the wear due to the substrate surface structure becoming unstable after corrosion, the plastic deformation layer is destroyed by corrosion, and the wear pit area increases after the corrosion and friction interaction test, which results in having the maximum wear rate[16].

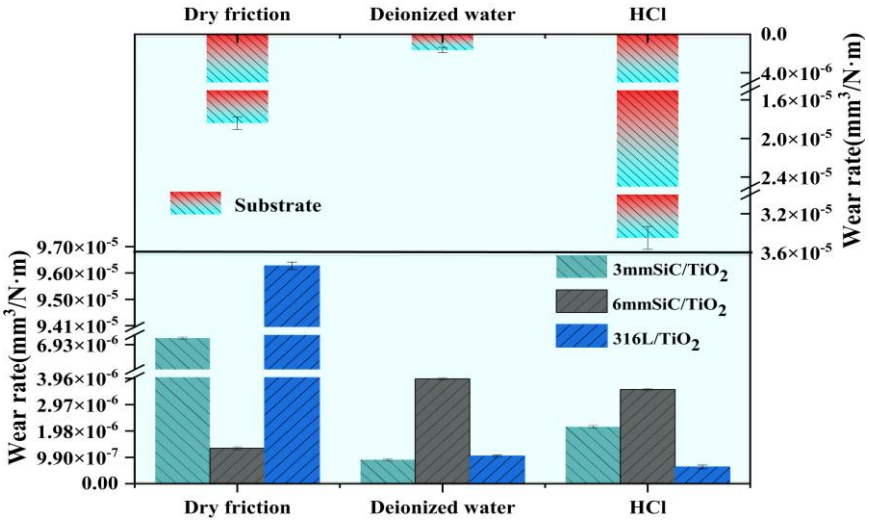

Figure 5: Wear rate of coatings and substrates in different environments

3.4.2. Counterpart ball wear rate

Figure 6 shows the wear rate data for the balls in different environments. As can be seen from

the figure, the difference in wear volume between the counterpart balls in dry friction and deionised water environments is very small. Specifically, the wear volumes of 3 mm SiC balls in dry friction and deionised water environments are 6.69×10^{-5} mm ³and 5.42×10^{-5} mm ³, respectively; and the wear volume of 6 mm SiC balls in dry friction and deionised water environments is 2.70×10^{-5} mm ³, respectively. In the hydrochloric acid environment, the wear volumes were 2.70×10^{-3}mm ³and 2.24×10^{-3} mm ³, respectively. In the hydrochloric acid environment, the wear volume of 3 mm SiC ball is 5.246×10^{-5} mm ³and 6 mm SiC ball is 6.95×10^{-5} mm ³.

In the dry friction and hydrochloric acid environments, the wear volume of the lower hardness 316L stainless steel ball is much higher than that of the SiC ball, 7.63×10^{-2} mm ³and 7.11×10^{-3} mm ³, respectively. This is due to the fact that the abrasive debris generated by the friction between the 316L stainless steel and the coating tends to adhere to the surface of the coating, leading to direct metal-to-metal wear, which is consistent with the high coefficient of friction phenomenon mentioned earlier. In contrast, in the deionised water environment, the 316L stainless steel ball had a wear volume of 1.48×10^{-3} mm ³, which is significantly lower than the wear rate in the dry friction and hydrochloric acid environments.

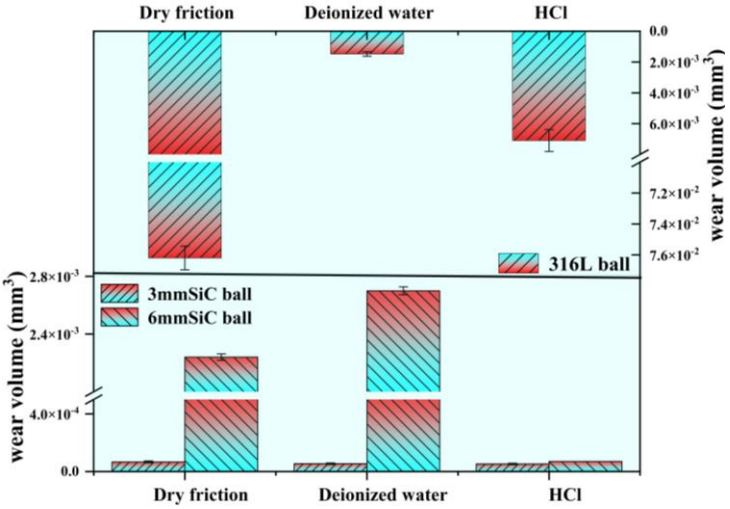

Figure 6: Wear volume of balls in different environments

3.5. Coating abrasion morphology analysis

Figures 7 and 8 present the wear scar morphology of TiO_2 coatings, the worn spot morphology of 3mm SiC counterpart balls, and their corresponding EDS spectra under different environmental conditions. In the dry friction and deionised water environments, the abrasion marks of the coating and the main wear mechanism of the counterpart balls are abrasive wear, while the coating surface also shows exfoliation. This is due to the large contact stresses causing the hard particles exfoliated from the coating surface to have a ploughing effect on the coating and the surface of the dyadic balls, which exacerbates the wear. In the HCl environment, there were obvious plough grooves on the surface of the wear marks of both the counterpart ball and the coating, and the surface of the wear marks was rough, indicating that the main wear mechanism was still abrasive wear.

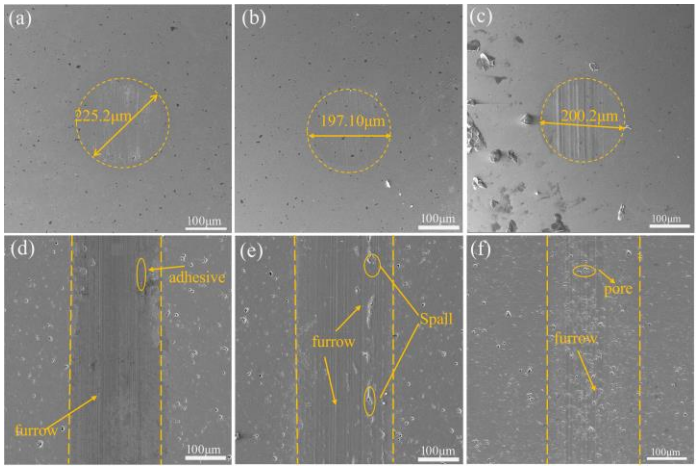

Figure 7: SEM abrasion morphology of 3 mm SiC counter-abrasive TiO_2 coating and pairs in different environments (a)(d) Dry friction environment (b)(e) Deionised water environment (c)(f) HCl environment

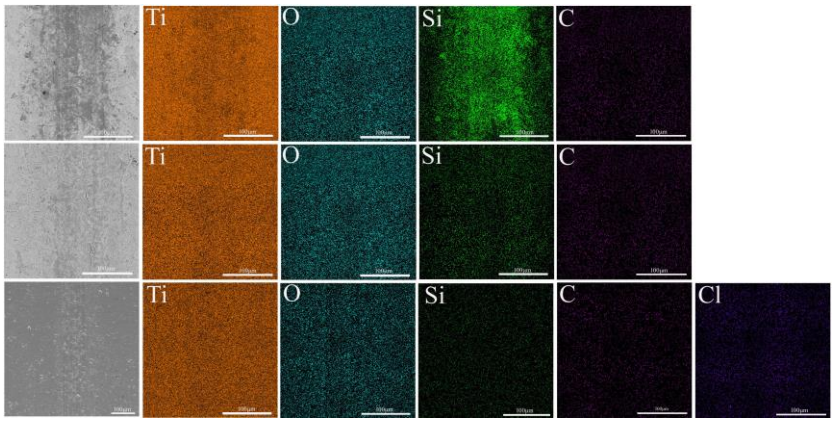

Figure 8: EDS spectra of abrasion marks of 3 mm SiC counter-abrasive TiO_2 coatings under different environments

Figure 9 demonstrates the morphology of the wear marks of the TiO_2 coating with 6 mm SiC balls in different environments. In the dry friction and deionised water environments, the surface of the wear area of the counterpart ball is very smooth, indicating that the main wear mechanism is typical polishing wear[17]. In the dry friction environment, the surface of the coated wear marks showed an adhesion phenomenon, which could be attributed to the formation of a thin film by the reciprocal extrusion of abrasive debris generated by the SiC balls during the counter-abrasion process[18]. The EDS analysis shows that the main components of the adhesion are Si and O elements. In the deionised water environment, the lubricating film formed by water molecules made the surface of the abrasive mark smoother, further reducing the wear.

In the HCl environment, the wear of SiC on the coupled balls is more slightly, with only shallow furrows present, and there was almost no significant difference between the wear mark surface of the TiO_2 coating and the unworn area. This is due to the fact that the load and friction are uniformly distributed on the smooth ceramic surface, creating a larger true contact area, which reduces the generation of microcracks, avoids stress concentration in the coating, and ultimately results in a smooth morphology on the wear scar surface[19].

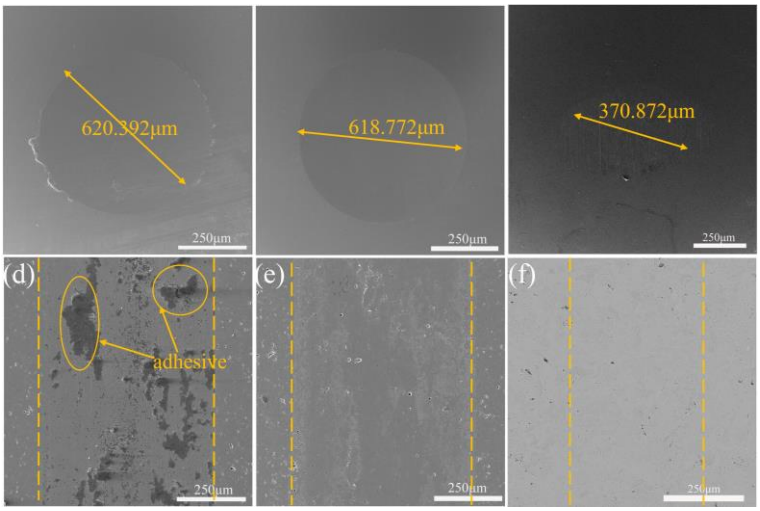

Figure 9: SEM abrasion morphology of 6 mm SiC counter-abrasive TiO2 coating and pairs in different environments (a)(d) Dry friction environment (b)(e) Deionised water environment (c)(f) HCl environment

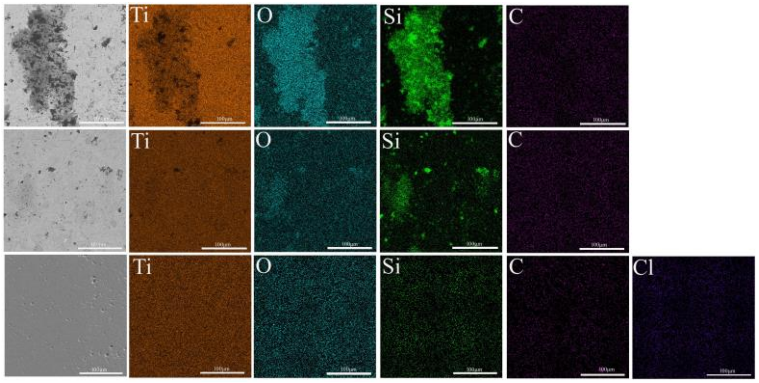

Figure 10: EDS spectra of abrasion marks of 6 mm SiC counter-abrasive TiO2 coatings under different environments

Figure 11 illustrates the abrasion morphology and pairwise wear morphology of the TiO_2 coating and the 316L counterpart ball in different environments. In the dry friction environment, the wear of the counterpart ball and the coating is the most serious. There are obvious plough furrows on the surface of the 316L counterpart ball, which is due to the existence of micro-bumps in the friction contact area of the coating, and these micro-bumps are smoothed out or dislodged during friction and the dislodged abrasive particles produce ploughing effect on the surface of the 316L ball, which indicates that the wear mechanism at this time is mainly abrasive wear. From the high magnification photos, it can be seen that the surface roughness of the coating abrasion marks is large, and there is a large area of flaking phenomenon. EDS analysis of the inside of the abrasion marks revealed that Fe oxides adhered to the surface of the coating, and compaction and tearing phenomena occurred during reciprocal friction, indicating that the wear mechanism of the coating in the dry friction environment was dominated by adhesive wear.

In the deionised water environment, the 316L couples showed the least wear of the three environments with a smooth wear spot surface. The presence of deionised water significantly reduced the hard abrasive particles inside the wear marks, creating an abrasive polishing effect of the coating on the 316L balls. Compared to a dry friction environment, there is only a small amount of abrasive debris within the coated abrasions and the abrasive roughness of the abrasions is less. According to EDS analysis, Fe oxides were still present inside the wear marks, but their mass

percentage was lower than that in the dry friction environment, indicating that the presence of deionised water effectively reduced the occurrence of adhesive wear.

During friction in HCl medium, the 316L ball were more susceptible to ploughing by abrasive chips and hard particles due to severe corrosion, leading to a synergistic effect of corrosive and abrasive wear. However, the inside of the coated abrasion marks was smooth and there were no obvious wear marks. EDS analysis showed that Ti elements were uniformly distributed on the surface of the abrasion marks and the mass percentage of Fe elements was very low, and almost no adhesion phenomenon was observed. This is due to the corrosive effect of HCl that makes the abrasive chips adhering to the coating easier to be sheared during friction, making it difficult to form adhesion on the coating surface, and thus the pair of balls formed a polishing effect on the coating.

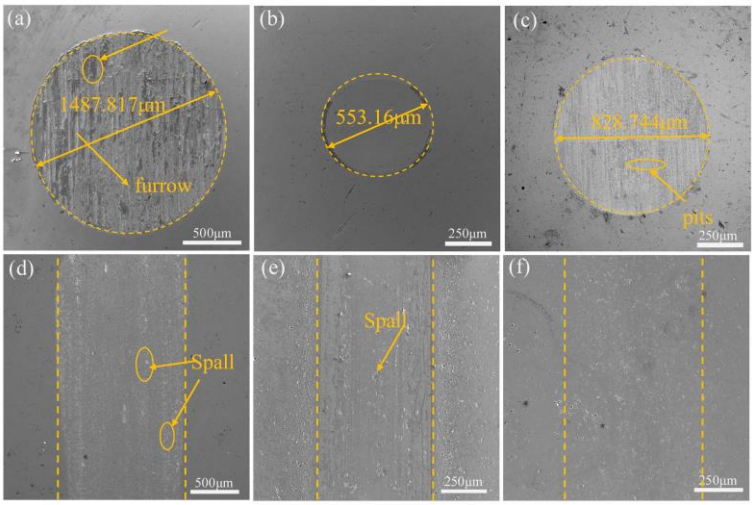

Figure 11: SEM abrasion morphology of 6mm 316L counter-abrasive TiO2 coating and pairs in different environments (a)(d) Dry friction environment (b)(e) Deionised water environment (c)(f) HCl environment

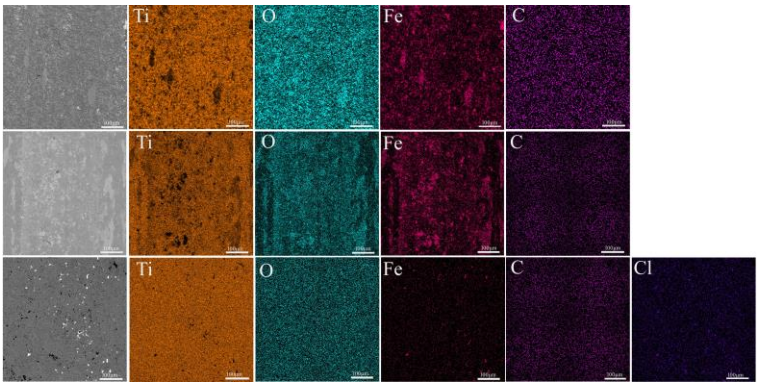

Figure 12: EDS spectra of abrasion marks of 6 mm SiC counter-abrasive TiO_2 coatings under different environments

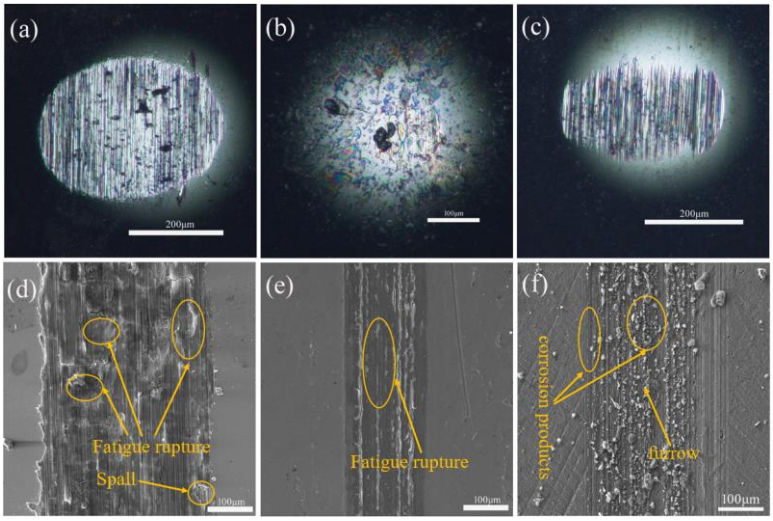

Figure 13: SEM abrasion morphology and pairwise abrasion photomicrographs of 3mm SiC butt-ground 310S substrate in different environments (a)(d) Dry friction environment (b)(e) Deionised water environment (c)(f) HCl environment

Figure 13 demonstrates the morphology of the wear marks of the counterpart balls and the substrate, the counterpart balls were severely worn in the dry friction, HCl environment, the wear marks have distinctive furrows, and the main wear is abrasive wear. In the deionised environment, the counterpart balls were only slightly worn. In the dry friction environment, the substrate underwent plastic deformation and was compacted, and the metal eventually underwent fatigue fracture and spalling as cyclic compressive and shear stresses were applied. In the deionised water environment, the wear marks were the narrowest and there were fewer internal abrasive chips, indicating that deionised water reduced abrasive wear to some extent, but severe fatigue wear and spalling still occurred. In contrast, in the HCl medium, reciprocating friction exacerbated the corrosion of the metal, and the interior of the wear marks was filled with corrosion products and showed traces of plough furrows, with the main wear mechanisms being corrosive wear and abrasive wear.

3.6. Corrosion behaviour of TiO_2 coatings and substrates under 5% HCl

Open Circuit Potential (OCP) measurement is a simple yet effective technique that provides critical information regarding the electrochemical state of worn metallic surfaces. The OCP measured during tribocorrosion tests reflects the relative electrochemical state between worn and unworn regions. This mixing potential is influenced by a number of factors, including the kinetics of the anodic and cathodic reactions, the relative proportions and distribution of the worn and unworn regions, and the OCP inherent of the materials in these regions [20].

During substrate OCP measurement, the samples were first immersed for 300 seconds to observe the state before friction began. The results are shown in Fig. 14(a), where the OCP decreases slightly with time, indicating that the substrate is being subjected to a corrosive medium. When friction started, the OCP of the substrate rapidly increased and stabilised at about -0.2 V at 310 s. After the end of friction, the OCP rapidly decreased to -0.27 V. The coating exhibited unstable OCP variations during the initial 300-second immersion period due to the presence of micro-pores and cracks in the coating. However, after the commencement of tribological testing, the OCP abruptly increased and stabilized at -0.32 V, followed by a decrease to 0.42 V upon friction termination. The positive shift of the OCP indicates that the coating and the substrate did not form an effective passivation film, or the passivation film formed was not sufficiently stable and exhibited passivation

effects only under specific conditions[21]. The potential difference that may exist between the coating and substrate and the SiC spheres during friction may lead to the formation of tiny macro-cells. SiC may induce the formation of localized potential differences, thereby reducing the electrochemical corrosion rate in these regions and shifting the OCP toward more positive values.

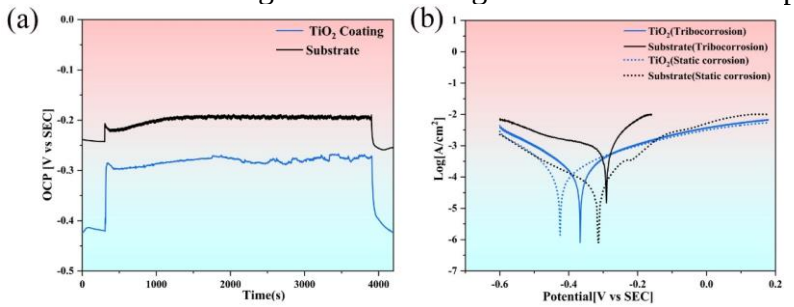

Figure 14: Open-circuit voltage and tafel curves for coating and substrate in 5% HCl environment (a) Open-circuit voltage for coating and substrate (b) Dynamic and static tafel curves for coating and substrate

The results of the static corrosion tests are shown in Fig.14(b), where the coating maintains a stable current in the cathodic and anodic regions without passivation, while the substrate reaches a local corrosion potential at a stable current with an anodic potential of -0.219V. Under friction conditions, the electrochemical behaviours of the coating and the substrate converge, with the corrosion potential shifted to the anodic region. This suggests that the corrosion kinetics in the wear marks differed from those in the unworn region, and that the sliding contact hindered the natural progression of the corrosion process and slowed down the corrosion rate in the wear marks.

By analysing the static and dynamic potential curves of the titanium oxide coating and the 310S substrate, we calculated the corrosion current density (I_{corr}) and corrosion potential (E_{corr}) from the polarisation curves using the Tafel extrapolation method. Among them, Icorr is a kinetic parameter reflecting the corrosion rate, and materials with lower Icorr usually have stronger corrosion resistance; while E_{corr} is a thermodynamic parameter reflecting the tendency and likelihood of corrosion occurring, which is directly proportional to the corrosion resistance of the material [22].The static corrosion current density of the TiO_2 coating was 1.267×10^{-4} A/cm ²and the dynamic corrosion current density is 1.705×10^{-4} A/cm ². The static corrosion current density of the substrate was 1.470×10^{-4} A/cm ² and the dynamic corrosion current density was 1.223×10^{-3}A/cm ². The dynamic and static corrosion potentials of the substrate were -0.291V and -0.314V, respectively, while those of the TiO_2 coating were -0.423V and -0.366V, respectively. Generally, the more positive the corrosion potential, the lesser the corrosion current density, which indicates the better the corrosion resistance of the material. The corrosion potential of the substrate is slightly higher than that of the coating, which is attributed to the inherent pore and microcrack defects in the thermally sprayed ceramic coating, resulting in a relatively more negative corrosion potential.

To further investigate the corrosion state of the 310S substrate and TiO_2 ceramic coating in 5% HCl solution, we compared them by electrochemical impedance spectroscopy (EIS) and the corresponding Nyquist and Bode plots. In the Nyquist plots, the presence of a distinct semicircle usually indicates the presence of electrochemical processes, such as charge transfer processes. A larger diameter of the semicircle indicates a higher impedance to the electrochemical reaction and a higher corrosion resistance[23]. The results show that the impedance of the substrate is slightly higher than the impedance of the coating. The Bode plots of the impedance at different frequencies show an increase with decreasing frequency and show a single peaked phase angle in the low frequency region, with a maximum phase angle of -45 °.

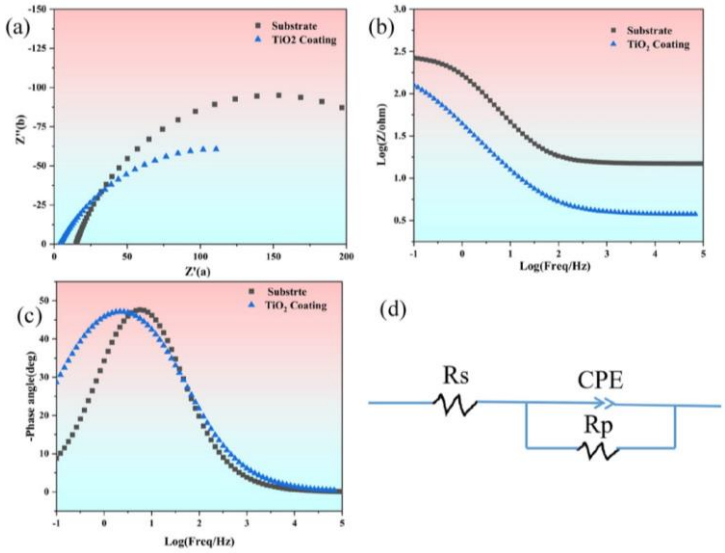

Figure 15: Open-circuit voltage and tafel curves for coating and substrate in 5% HCl environment (a) Open-circuit voltage for coating and substrate (b) Dynamic and static tafel curves for coating and substrate

The equivalent circuit was used to simulate the sample/solution interface and interpret the EIS data using ZView2 software, and the equivalent circuit diagram is shown in Fig.15(d). Rs is the solution resistance, Rp represents the charge transfer resistance of the coating, and CPE represents the capacitance, which yields a substrate impedance of 270.1Ω·cm^2, and the impedance of the titanium oxide coating is 237Ω·cm^2. In summary, it can be learnt that, after being coated by plasma spraying, the presence of the coating has little effect on the corrosion resistance of the substrate.

4. Conclusions

In friction experiments, it was found that the lower hardness 316L counter-abrasive balls instead gave the coating the highest wear rate under dry friction and de-ionised water, and the counter-abrasive balls themselves wore heavily. When the hardness SiC balls were rubbed against the coating, the coating showed excellent wear resistance at both high and low contact stresses. The wear rate of the balls was less than that of the 316L balls in both dry friction and HCl. In HCl, the static and dynamic potential profiles of the TiO_2 coatings were more negative than those of the 310s substrate, but the coatings had lower corrosion current densities. the coating was still effective in slowing down the penetration of corrosive ions, decreasing the corrosion current density, and enhancing the corrosion resistance.

Acknowledgment

This work was supported by the National Natural Science Foundation of China (52305205) and Natural Science Basic Research Program of Shaanxi (Program No. 2022JQ-477).

References

[1] Wang Qiang, Wang Huanhuan, Yuan Shuo, et al. Research Progress on Service Damage and Protection of Slipper Pair in Axial Piston Pump [J]. Surface Technology, 2023, 52(06): 126-139.
[2] LIU Er-Yong, ZENG Zhi-Xiang, ZHAO Wen-Jie. Research progress of integrated technology for corrosion and wear of metallic materials and wear and corrosion resistance in seawater environment [J]. Surface Technology, 2017, 46(11): 149-157.

[3] LóPEZ-ORTEGA A, BAYóN R, ARANA J L, et al. Influence of temperature on the corrosion and tribocorrosion behaviour of High-Strength Low-Alloy steels used in offshore applications [J]. Tribology International, 2018.
[4] BENLI B, CELIK I. Surface Modification and Analysis of St37 Steel with Al2O3-TiO2, ZrO2, and Cr2O3 Ceramic Coatings: Structural, Mechanical, and Tribological Properties [J]. Tribology International, 2023.
[5] MEDVEDOVSKI E. Special Issue: 'Advanced Ceramics and Coatings for Wear and Corrosion Applications' [J]. Advances in Applied Ceramics, 2023.
[6] KHADEM M, PENKOV O V, YANG H-K, et al. Tribology of multilayer coatings for wear reduction: A review [J]. Friction, 2017.
[7] Li Changjiu. Thermal spraying technology application and research progress and challenges [J]. Thermal Spraying Technology, 2018, 10(04): 1-22.
[8] SALIMIJAZI H, HOSSEINI M, MOSTAGHIMI J, et al. Plasma Sprayed Coating Using Mullite and Mixed Alumina/Silica Powders [J]. Journal of Thermal Spray Technology, 2012.
[9] WANG Chengpeng, WU Xiaobo, XIAO Yexiang, et al. Friction and Wear Behaviour of Alumina Ceramics and Corrosion-Resistant Metals under Different Environmental Media [J]. Lubrication and Sealing, 2021, 46(04): 1-5+11.
[10] XIAO J-K, WU Y-Q, ZHANG W, et al. Microstructure, wear and corrosion behaviors of plasma sprayed NiCrBSi-Zr coating [J]. Surface & Coatings Technology, 2019.
[11] HASHEMI S M, PARVIN N, VALEFI Z, et al. Comparative study on tribological and corrosion protection properties of plasma sprayed Cr2O3-YSZ-SiC ceramic coatings [J]. Ceramics International, 2019.
[12] Ma Fengxiao, Guo Xingye, He Hanwei, et al. Preparation of plasma sprayed high strength nano TiO2 coating and its mechanical properties [J]. Thermal Spraying Technology, 2024, 16(02): 99-105+12.
[13] XU J, ZHANG C, SUN G, et al. Role of SiC nanoparticles on tribological properties of atmospheric plasma sprayed 5 wt% SiC–Ni60 coatings [J]. Tribology International, 2020.
[14] Pei Bingbing, Pei Wenle, Wang Jianmei, et al. Corrosion and wear behaviour of Q345 steel in artificial seawater [J]. Lubrication and Sealing: 1-8.
[15] LóPEZ A, BAYóN R, PAGANO F, et al. Tribocorrosion behaviour of mooring high strength low alloy steels in synthetic seawater [J]. Wear, 2015.
[16] SU X, XU G, ZHU M, et al. Investigation on the interaction between corrosion and wear of U68CuCr rail steel with different corrosion periods [J]. Wear, 2022.
[17] YAN Z, JIANG D, GAO X, et al. Friction and wear behavior of TiN films against ceramic and steel balls [J]. Tribology International, 2018.
[18] MATSUDA M, KATO K, HASHIMOTO A. Friction and Wear Properties of Silicon Carbide in Water from Different Sources [J]. Tribology Letters, 2011.
[19] LI S, XI X, HOU G, et al. Preparation of plasma sprayed mullite coating on stainless steel substrate and investigation of its environmental dependence of friction and wear behavior [J]. Tribology International, 2015.
[20] TEKIN K C, MALAYOGLU U. Assessing the Tribocorrosion Performance of Three Different Nickel-Based Superalloys [J]. Tribology Letters, 2009.
[21] ZHANG B, WANG J, LIU H, et al. Tribocorrosion properties of AISI 1045 and AISI 2205 steels in seawater: Synergistic interactions of wear and corrosion [J]. Friction, 2020.
[22] WU H, WANG L, ZHANG S, et al. Tribological properties and sulfuric acid corrosion resistance of laser clad CoCrFeNi high entropy alloy coatings with different types of TiC reinforcement [J]. Tribology International, 2023.
[23] LIU C, BI Q, MATTHEWS A. EIS comparison on corrosion performance of PVD TiN and CrN coated mild steel in 0.5 N NaCl aqueous solution [J]. Corrosion Science, 2001.